Clinical Cancer Research

Entinostat Neutralizes Myeloid-Derived Suppressor Cells and Enhances the Antitumor Effect of PD-1 Inhibition in Murine Models of Lung and Renal Cell Carcinoma

Ashley Orillion[1,2], Ayumi Hashimoto[3], Nur Damayanti[1], Li Shen[4], Remi Adelaiye-Ogala[1,5], Sreevani Arisa[1], Sreenivasulu Chintala[1], Peter Ordentlich[6], Chingai Kao[7], Bennett Elzey[7,8], Dmitry Gabrilovich[3], and Roberto Pili[1,7]

Abstract

Purpose: Recent advances in immunotherapy highlight the antitumor effects of immune checkpoint inhibition despite a relatively limited subset of patients receiving clinical benefit. The selective class I histone deacetylase inhibitor entinostat has been reported to have immunomodulatory activity including targeting of immune suppressor cells in the tumor microenvironment. Thus, we decided to assess whether entinostat could enhance anti–PD-1 treatment and investigate those alterations in the immunosuppressive tumor microenvironment that contribute to the combined antitumor activity.

Experimental Design: We utilized syngeneic mouse models of lung (LLC) and renal cell (RENCA) carcinoma and assessed immune correlates, tumor growth, and survival following treatment with entinostat (5 or 10 mg/kg, p.o.) and a PD-1 inhibitor (10 and 20 mg/kg, s.c.).

Results: Entinostat enhanced the antitumor effect of PD-1 inhibition in two syngeneic mouse tumor models by reducing tumor growth and increasing survival. Entinostat inhibited the immunosuppressive function of both polymorphonuclear (PMN)- and monocytic-myeloid derived suppressor cell (M-MDSC) populations. Analysis of MDSC response to entinostat revealed significantly reduced *arginase-1*, *iNOS*, and *COX-2* levels, suggesting potential mechanisms for the altered function. We also observed significant alterations in cytokine/chemokine release *in vivo* with a shift toward a tumor-suppressive microenvironment.

Conclusions: Our results demonstrate that entinostat enhances the antitumor effect of PD-1 targeting through functional inhibition of MDSCs and a transition away from an immune-suppressive tumor microenvironment. These data provide a mechanistic rationale for the clinical testing and potential markers of response of this novel combination in solid tumor patients. *Clin Cancer Res; 23(17); 5187–201.* ©2017 AACR.

Introduction

Momentum in the field of cancer immunotherapy has been significantly accelerating as several durable and effective cancer treatments based on promoting an antitumor immune response are now available for patients with solid tumors, including renal cell carcinoma (RCC) and non–small cell lung cancer (NSCLC). The PD-1/PD-L1 axis plays a central role in the immune evasion capability of tumor cells by hampering the antitumor activity of cytotoxic T cells. Blocking these immune checkpoints, which have been reported as being aberrantly expressed on solid tumors such as RCC and NSCLC, has recently led to the approval of nivolumab, pembrolizumab, and atezolizumab in these diseases (1–4). However, despite these significant clinical advances, the clinical benefits of immunotherapies for RCC and NSCLC are restricted to a subset of patients. Tumor escape due to immune tolerance and an immunosuppressive tumor microenvironment (TME) represents a major obstacle in maximizing the full clinical potential of immune checkpoint inhibitors both in the indications where they have shown activity and in expanding to tumor types where these agents have not been as effective.

Entinostat is an oral, class I–specific histone deacetylase inhibitor (HDACi) shown to disrupt the dynamic interactions between the TME and host immune surveillance (5, 6). Tumor cells classically avoid immune surveillance by releasing a plethora of immune-suppressive factors and chemoattractants

[1]Gentourinary Program, Simon Cancer Center, Indiana University, Indianapolis, Indiana. [2]Department of Cellular and Molecular Biology, University at Buffalo, Roswell Park Cancer Institute, Buffalo, New York. [3]The Wistar Institute, Philadelphia, Pennsylvania. [4]Department of Medicine, Roswell Park Cancer Institute, Buffalo, New York. [5]Department of Cancer Pathology and Prevention, University at Buffalo, Roswell Park Cancer Institute, Buffalo, New York. [6]Syndax Pharmaceuticals, Inc., New York, New York. [7]Department of Urology, Indiana University, Indianapolis, Indiana. [8]Center for Cancer Research, Purdue University, West Lafayette, Indiana.

Note: Supplementary data for this article are available at Clinical Cancer Research Online (http://clincancerres.aacrjournals.org/).

A. Orillion and A. Hashimoto contributed equally to this article.

Corresponding Authors: Roberto Pili, Indiana University, 535 Barnhill Drive, Indianapolis, IN 46202. Phone: 317-278-7776; Fax: 317-278-7776; E-mail: rpili@iu.edu; and Dmitry Gabrilovich, Translational Tumor Immunology, The Wistar Institute, Philadelphia, PA. E-mail: dgabrilovich@wistar.org

doi: 10.1158/1078-0432.CCR-17-0741

Translational Relevance

Despite the significant progress achieved with PD-1/PD-L1 inhibitors in the treatment of solid tumors, the majority of patients still present with progressive disease following these agents. Resistance to immune checkpoint inhibitors may in part be mediated by an immunosuppressive tumor microenvironment. Here we report that this suppressive microenvironment can be altered with entinostat treatment in two distinct preclinical tumor models to enhance the antitumor efficacy of PD-1 targeted therapy. Therefore, we identified an effective combination strategy with anti–PD-1 inhibition and entinostat that is being readily translated to patients with solid tumors, including lung and renal cell carcinoma.

enabling tumor-promoting inflammation (7). HDAC inhibitors can increase immunogenicity of tumor cells by activating expression of tumor antigen, antigen presentation, and costimulation molecules in tumor cells (6, 8). In addition, our group has shown that entinostat synergistically enhances IL2 immunotherapy in the RENCA model by inhibiting the function of immunosuppressive regulatory T cells (Treg) through acetylation of the STAT3 transcription factor (5). Entinostat is currently in clinical development for breast and lung cancer in combination therapies.

Myeloid-derived suppressor cells (MDSC) represent a highly immunosuppressive population of tumor-infiltrating immature myeloid cells. These cells contribute to tumor immune escape by inhibiting cytotoxic T-cell proliferation and driving Treg induction (3, 9, 10). Recent studies have reported that *in vitro* pan-HDAC inhibition may influence MDSCs to a more differentiated status of macrophage or dendritic cell (DC; 6, 8, 11). Alternatively, another study treating bone marrow precursor cells with pan-HDAC inhibitors resulted in the expansion of monocytic MDSC populations (6, 8, 12). Interestingly, a combination of demethylating agent and HDAC inhibitor enhanced the antitumor effect of combined PD-1 and CTLA-4 inhibition in colon and breast cancer models, and was associated with decreased MDSCs (13).

In this study, our aim was to further understand the mechanistic basis for how entinostat targeting of MDSCs and alteration of the immunosuppressive TME leads to enhanced immune checkpoint inhibitor antitumor activity. We conducted preclinical studies of entinostat in combination with anti–PD-1 antibody treatment in two syngeneic mouse models, RENCA and Lewis lung carcinoma (LLC), and assessed the effect of single agents and the combination on immune relevant endpoints. Our *in vivo* results, which we subsequently confirmed using *in vitro* mechanism-based assays, demonstrate that the significant antitumor activity of entinostat combined with anti–PD-1 is associated with a direct impact of entinostat on blocking the function of immunosuppressive tumor-infiltrating MDSCs. Our characterization of entinostat-mediated changes in enzymes, cytokines, chemokines, and other growth factors associated with an immunosuppressive TME offers multiple candidates to serve as potential biomarkers for ongoing clinical trials. We believe our data further support the importance of targeting MDSC function to enhance immune checkpoint blockade and significantly advance the mechanistic rationale for the clinical testing of entinostat combined with PD-1/PD-L1–targeted therapies.

Materials and Methods

Cell lines

The RENCA-Luc murine RCC cell line, purchased from the American Type Culture Collection (ATCC, National Cancer Institute), was stably transfected with a luciferase reporter in the Pili laboratory. Cells were cultured using RPMI 1640 (Corning) with 10% FBS (Corning) and 1% pen/strep (Life Technologies). Cells were incubated in an incubator maintained at 37°C and 5% CO_2. Confluent cells (75%–80%) were harvested for orthotopic injection into the kidney of Balb/c mice using 0.25% Trypsin (Corning) and suspended in a 1:1 ratio of Matrigel (Corning) and DPBS (Gibco). LLC lung carcinoma and CT26 colon carcinoma were obtained from the ATCC and cultured in DMEM (Corning Incorporated) supplemented with 10% FBS (Atlanta Biologicals, Inc.) and 1% antibiotics (Thermo Fisher Scientific Inc.). The cells were harvested using 0.25% Trypsin (Thermo Fisher Scientific Inc.), suspended in DPBS (Corning) as 200 μL containing 5×10^5 cells, and injected s.c. into the mice. After tumors were established, the mice were randomized into 2 groups and orally treated with 10 mg/kg of entinostat daily. The J774M cell line was kindly provided by Georgia Cancer Center (Dr. Kebin Liu) and cultured with DMEM (Corning) media with 10% FBS (Corning) and 1% pen/strep (Life Technologies). Cells were incubated in a 37°C and 5% CO_2. Confluent cells (70%–80%) were harvested using a cell scraper and passaged as suggested for the parent cell line via the ATCC guidelines.

Hematopoietic progenitor cells culture

Lineage-negative cells were purified from C57BL/6-naïve bone marrow cells using the lineage cell depletion Kit (Miltenyi). Naïve bone marrow cells were subsequently treated with biotinylated antilineage antibody and antibiotin microbeads, and passed through the MACS column according to the manufacturer's instruction. Lineage-negative cells were cultured in RPMI (Corning Incorporated) supplemented with 10% FBS, 1% antibiotics, and 50 μmol/L 2-mercaptoethanol (Thermo Fisher Scientific Inc.) with 20 ng/mL of recombinant GM-CSF (Invitrogen), at 50,000 cells/well in 24-well plates. Tumor explant supernatants (TES) were obtained by culturing small pieces of EL4 tumors with complete RPMI media for 24 hours. On day 1, TES or media with DMSO or entinostat solution were added into the wells at 10% to get the final concentration of 100 or 500 nmol/L entinostat. On day 3, the half of culture supernatant was exchanged to fresh media supplemented with 20 ng/mL of GM-CSF with or without 10% TES. On day 6, the cells were collected and analyzed by flow cytometric analysis, or used for functional analysis.

Tumor, bone marrow, and spleen cells isolation

Live tumor sections were isolated from tumors, cut into small pieces, and digested with an enzyme cocktail solution from the mouse tumor dissociation Kit (Miltenyi Biotec—130-096-730). Tumors were incubated with the enzyme cocktail for 30 minutes at 37°C with agitation. The enzyme reaction was arrested using PBS, cells were spun at 300 *g*, 4°C for 7 minutes, resuspended in PBS, and mashed through a 70 μm cell strainer.

Cells from these tumors were either used for flow cytometry analysis or further processed and used for functional analyses. Whole spleens and bone marrow were harvested from mice and processed into single-cell suspensions. Cells were then washed, lysed with red blood cell lysis buffer (Affymetrix 00-4333-57) or using ammonium chloride lysis buffer, and cultured in RPMI medium with 10% FBS, Pen (100 units/mL)–Strep (100 mg/mL), 1 mmol/L sodium pyruvate, 100 mmol/L non-essential amino acids, 2 mmol/L L-Glutamine, and 55 μmol/L BME, with anti-CD3 (eBioscience 16-0031-85) and anti-CD28 (eBioscience 5012503) antibodies for approximately 24 hours. $CD8^+$ T cells were then isolated using a $CD8a^+$ T-cell isolation kit from Miltenyi Biotec (130-104-075), stained with carboxyfluorescein succinimidyl ester (CFSE; NC9759757), per the manufacturer's protocol, and cocultured with MDSCs as described below.

MDSC isolation and T-cell suppression assay

MDSCs were isolated from tumors using the Miltenyi Biotec's Myeloid Derived Suppressor Cell Isolation Kit (130-094-538) and cocultured with isolated $CD8^+$ T cells in serially diluted concentrations. T cells (1×10^5; isolated with a $CD8a^+$ T-cell isolation kit; Miltenyi Biotec) were cultured in plates with varying numbers of either PMN-MDSCs or M-MDSCs isolated from RENCA tumors for 16 to 18 hours. T cells isolated in the listed method were cocultured with entinostat-treated J774M cells for 68 to 72 hours. Cells were then harvested, stained, and analyzed via FACS analysis.

In vivo treatment

All procedures were performed and approved in strict accordance with the Institutional Animal Care and Use Committee at Roswell Park Cancer Institute, Indiana University School of Medicine, Wistar Institute, and with the NIH Guide for the Care and Use of Laboratory Animal guidelines. Female 5- to 6-week-old Balb/c and C57BL/6 mice (Charles River Labs) were maintained in a temperature-controlled room with a 12/12-hour light/dark schedule and food provided *ad libitum*. Confluent RENCA-Luc cells (70%–80%) were harvested using 0.25% Trypsin (Corning) and suspended in a 1:1 ratio of Matrigel (Corning) and HBSS (Gibco), and 10 μL containing 1×10^4 cells was injected under the renal capsule. One week postinjection preliminary bioluminescence imaging was performed and mice were randomized into four groups: control, entinostat, anti–PD-1 (Bio X Cell RPM1-14, rat IgG2a), or a combination of entinostat and anti–PD-1. Mouse tumors were serially imaged using a bioluminescent IVIS imaging machine. LLC tumor–bearing mice were randomized into 4 groups ($n = 5$) on day 11 and orally treated with vehicle (1% DMSO) or entinostat solution (10 mg/kg) every day. Anti–PD-1 antibody (clone RMP1-14, Bio X Cell) or isotype control antibody (clone 2A3, Rat IgG2a, Bio X Cell) was i.p. administered on days 11, 14, 18, and 21. Mice in the treatment groups were treated orally with 5 mg/kg entinostat for 5 days/week, and with PD-1 inhibitor 10 or 20 mg/kg (second survival study) i.p. from BioXCell, or a combination treatment regimen.

Cell staining and flow cytometry

Splenocytes, tumor cell suspensions, and peripheral blood cells were washed, blocked with Fc Block (anti-mouse CD16/32 mAb; BD Biosciences) at 4°C for 15 minutes, and stained with fluorescence-conjugated antibodies against surface markers CD45(clone 30-F11), CD11b (clone M1/70), CD11c, Gr1 (clone RB6-8C5), Ly6C (clone AL-21), Ly6G (clone 1A8), F480 (clone BM8), I-Ab, I-Ad, CD8a (clone 53-6.7), and CD4 (clone RM4-5) antibodies purchased from BioLegend, eBioscience, or BD Biosciences. Cells were then fixed in a fixation/permeabilization buffer (eBioscience) and stained with antibodies against intracellular proteins, including FoxP3 (NRRF-30) and Granzyme B (clone GB11). The antibodies were purchased from BD Biosciences, Biolegend, and R&D Systems and used for staining. Lineage antibody cocktail was purchased from eBioscience. Anti-mouse CCR2 antibody was purchased from R&D Systems, Inc. Stained cells and isotype-control–stained cells were assayed using a LSRII, LSR4, or Fortessa flow cytometer (BD Biosciences). Data analysis was performed using the FlowJo (FlowJo LLC, Tree Star) and/or ModFit LT 4.1 software.

Proteome profile

Tumor tissue was homogenized in PBS-containing protease inhibitors. Following homogenization, Triton X-100 was added to a final concentration of 1%, frozen at −80°C, thawed, centrifuged as 10,000 *g* for 5 minutes, quantified, and assayed according to the manufacturer's protocol. Blood samples were collected from mice in each cohort, allowed to clot for 2 hours at room temperature, and centrifuged at 2,000 *g* for 15 minutes. Serum samples were frozen at −80°C until time of analysis at which time they were run according to the manufacturer's protocol. All samples were processed and run on the R&D Systems mouse XL cytokine array Kit (Ary028). Analyses were performed using HLImage++ QuickSpots Tool (Western Vision Software) and GraphPad Prism7.

Immunoprecipitation and Western blot analysis

J774M cells were treated with entinostat at 0.5, 0.75, or 1 μmol/L for 6 hours and harvested in nondenaturing lysis buffer. Cells were subjected to immunoprecipitation per the manufacturer's protocol (Abcam 206996). STAT3 antibody was applied to 350 μg of lysate in microcentrifuge tubes and placed on a rotary mixer overnight at 4°C. The next day, protein A/G Sepharose beads were applied, and the mixture was placed on the rotary mixer for 1 hour at 4°C. Following pull-down of STAT3, samples were subjected to gel electrophoresis on 4% to 20% precast mini-protean polyacrylamide gels (Bio-Rad) and transferred onto nitrocellulose membranes. Proteins of interest were detected using acetylated lysine (1:1,000; Cell Signaling 9441S) and STAT3 (1:1,000, Cell Signaling 12640S). After incubation with conjugated secondary antibodies (Bio-Rad), membranes were exposed to chemiluminescence according to the manufacturer's instructions (Thermo Fisher Scientific) and exposed to film. Quantitative measurements were performed using ImageJ and GraphPad (Prism 7) software.

Quantitative real-time PCR

mRNA was extracted from J774M cells that were treated ± entinostat using standard Trizol protocols or using the total RNA extraction Kit (Omega Bio-tek). RNA concentration and purity were determined through measurement of A260/280 ratios with a Synergy Hi Multi-Mode reader. cDNA was prepared using the iScript Kit (Bio-Rad) or the cDNA reverse transcriptase Kit (Applied Biosystems), and qPCR was performed in

triplicate for each sample using SYBR Master Mixture (Bio-Rad or Applied Biosystems). Samples were run on an Applied Biosystems 7900HT fast real-time PCR system. Sequence Detection Systems software v2.3 was used to identify the cycle threshold (C_t) values and to generate gene expression curves. Data were normalized to Gapdh expression and fold change was calculated. The primers used for target genes were: *Gapdh* 5′-AACTTTGGCATTGTGGAAGG-3′ and 5′-ACACATTGGGGGTAGGAACA-3′; *iNOS*, 5′-AACGGAGAACGTTGGATTTG-3′ and 5′-CAGCACAAGGGGTTTTCTTC-3′; *Arg1*, 5′-GCTGTCTTCCCAAGAGTTGGG-3′ and 5′-ATGGAAGAGACCTTCAGCTAC-3′; COX-2, 5′-CCAGCACTTCACCCATCAGTT-3′ and 5′-ACCCAGGTCCTCGCTTATGA-3′; and *Actb*, 5′-ATGGAGGGGAATACAGCCC-3′ and 5′-TTCTTTGCAGCTCCTTCGTT-3′. Expressions of the different genes were normalized to *Gapdh* or *Actb*. Relative expression was calculated using the $2^{-\Delta\Delta C_t}$ method

[sample calculation: 2^ − ((treated$_{target}$ − treated$_{actin/gapdh}$) − (average(control$_{target}$) − average(control$_{actin/gapdh}$)))]

NO production

Ly6G$^+$ cells from HPC culture were cocultured with naïve whole spleen cells and 0.1 μg/mL of anti-CD3 and CD28 antibodies for 24 hours. Nitrite concentration in culture supernatant was measured using Griess Reagent System (Promega).

Arginase activity

Ly6G$^+$ cells from spleen cells or HPC culture were lysed with the lysis buffer of the Arginase activity assay Kit (Abcam). Arginase activity of the cell lysates was measured using an Arginase activity assay kit. The arginase activity was normalized using the protein concentration which was detected by the Bradford dye-binding method using Bio-Rad Protein Assay Dye Reagent Concentrate (Bio-Rad Laboratories, Inc.).

PEG_2 production assay

Ly6G$^+$ cells from HPC culture were cultured at 2×10^6 cells/mL in RPMI complete media with 20 ng/mL of GM-CSF for 20 hours. PGE_2 concentration in supernatant was measured using the PGE_2 ELISA Kit (Invitrogen).

ROS staining

To determine the intracellular levels of ROS, spleen cells, tumor cells, and HPC culture cells were stained with antibodies against cell surface antigen and then incubated with DCFDA (Invitrogen) at 37°C for 30 minutes. The cells were analyzed by flow cytometry, and the mean fluorescence intensity of the ROS-reactive dichlorofluorescin was analyzed using FlowJo software.

Statistical analysis

All statistical analyses were performed using GraphPad Prism7 software for Windows. Analysis of survival was conducted using the Kaplan–Meier method. Differences in treatment group survivals were assessed with the log-rank test. All other statistical analyses in this study were performed between experimental groups using the Student *t* test with Welch's correction. A P value <0.05 was considered statistically significant.

Results

Entinostat enhances the antitumor effect of PD-1 inhibition in syngeneic mouse cancer models

We tested entinostat in combination with a mouse checkpoint inhibitor anti–PD-1 antibody in RENCA and LLC syngeneic mouse models of cancer. Both these models have been shown to attract highly immunosuppressive MDSCs to the TME, which play a key role in suppression of antitumor T-cell activity (14, 15). Balb/c or C57BL/6 mice were inoculated orthotopically with firefly luciferase-tagged RENCA cells or subcutaneously with LLC tumor cells, respectively. RENCA tumor–bearing mice were randomized based on bioluminescent readouts and separated into four groups: control, entinostat (5 mg/kg), anti–PD-1 (10 mg/kg), or the combination of entinostat and anti–PD-1. Treatment with entinostat alone resulted in significant inhibition of tumor growth across the studied models (RENCA: 52.6% growth inhibition; entinostat vs. control: $P = 0.0015$), whereas anti–PD-1 alone only moderately reduced tumor growth (35.05% growth inhibition; anti–PD-1 vs. control: $P = 0.0768$; Fig. 1A–C). The combination of entinostat and anti–PD-1 treatment was most effective in enhancing tumor growth inhibition compared with the control and each of the single treatment groups (83.3% reduction; combination vs. vehicle: $P < 0.0001$; combination vs. entinostat: $P = 0.0115$; combination vs. anti–PD-1: $P = 0.0076$; Fig. 1A–C).

Clinically, anti–PD-1 immunotherapy has shown prolonged stabilization of disease in approximately 40% of patients with RCC and lung cancer (1, 2, 16), leading to improvements in overall survival in these indications. Following the previous study in the RENCA model demonstrating tumor growth inhibition, we examined the survival outcome for the entinostat and anti–PD-1 antibody combination. Using the doses previously described, we observed a significant increase in survival for the combination treatment (combination vs. anti–PD-1: $P = 0.0012$; combination vs. control: $P = 0.0009$; Fig. 1E). Our results showed prolonged survival in the anti–PD-1 group and an enhanced effect in the combination-treated cohort also with increased dose of the PD-1 inhibitor (combination vs. control: $P = 0.0471$; combination vs. entinostat: $P = 0.0372$; Fig. 1F). To expand these observations to a different mouse model, we used LLC tumor–bearing mice. Mice were randomized at the time of appearance of palpable s.c. tumors. At the selected dose (10 mg/kg), entinostat as a single agent caused a modest but significant decrease in tumor growth. Similar decreases were observed in mice treated with PD-1 antibody alone. However, the combination of entinostat and anti–PD-1 resulted in significant reductions in tumor growth (Fig. 1D). The results of these studies demonstrate that the combination of entinostat with anti–PD-1 inhibits tumor growth in different tumor models.

Enhanced anti–PD-1 immunotherapy is associated with increased antitumor immune responses and decreased presence of immunosuppressive cell populations

To determine whether the inhibition of tumor growth resulting from the entinostat/anti–PD-1 combination treatment was associated with an enhanced immune response, we examined the circulating and tumor-infiltrating lymphoid and myeloid populations. Endpoint blood and tumor samples were collected from RENCA tumor–bearing mice and subjected to immunofluorescence staining and FACS analysis. We observed an

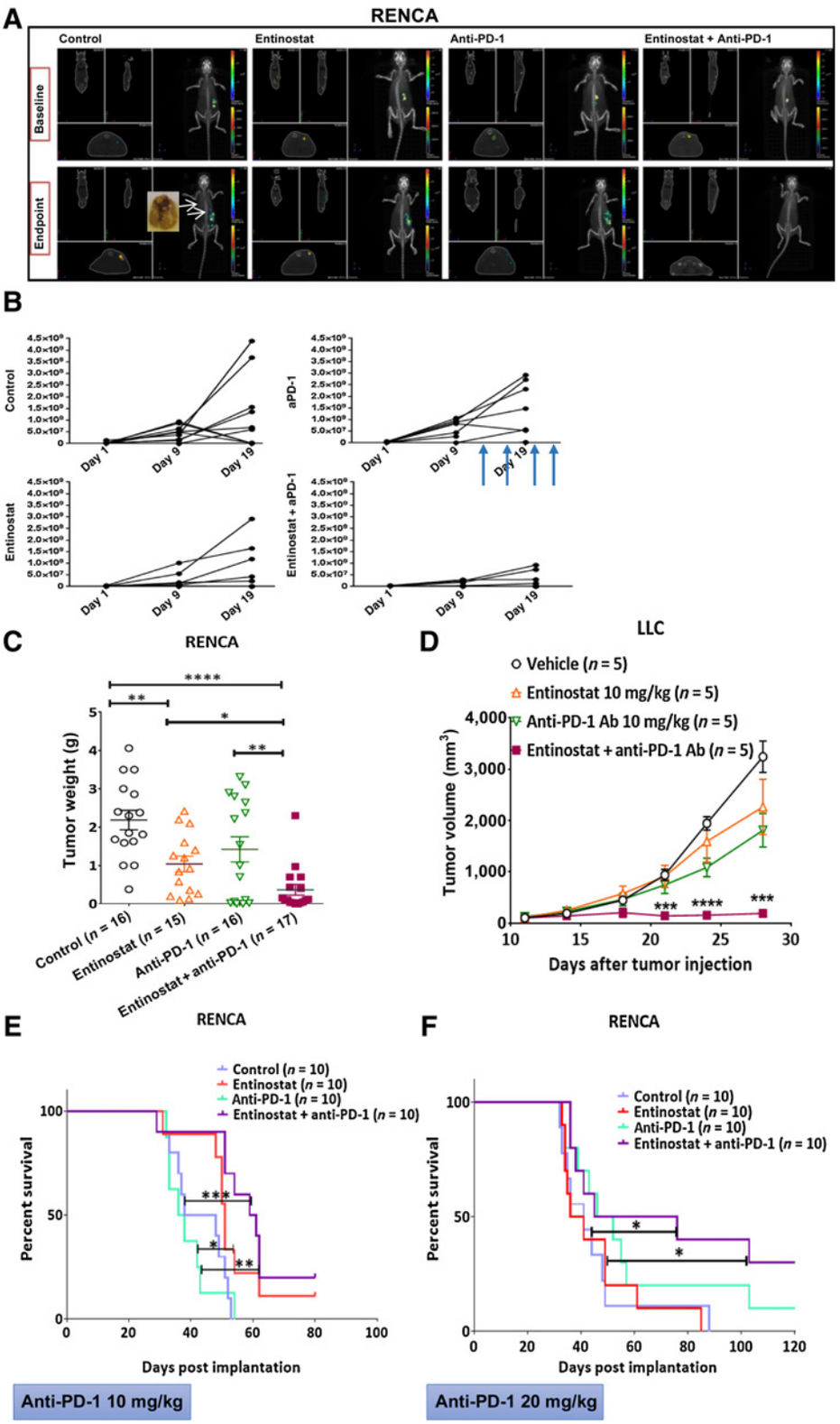

Figure 1.

Entinostat improves immunotherapy in syngeneic models of mouse of renal cell and lung carcinoma. **A–C, E–F,** RENCA model (**A**) Top: baseline bioluminescent imaging. Bottom: endpoint bioluminescent imaging. **B,** Average radiance [photons/second/centimeter squared/steradia] of each mouse in control, entinostat, anti–PD-1, and entinostat + anti–PD-1 cohorts across the duration of the study. (Top right) Arrows indicate the timepoints at which mice were treated with anti–PD-1: days 11, 14, 18, and 21. **C,** Endpoint tumor weight in grams. **D,** The LLC tumor–bearing mice were orally treated with vehicle (1% DMSO) or entinostat solution (10 mg/kg) from days 11 to 28. The mice were treated with anti–PD-1 antibody i.p. on days 11, 14, 18, and 21. **E,** Survival study, with 10 mg/kg of anti–PD-1. **F,** Survival study, with 20 mg/kg of anti–PD-1. Results are shown as mean ± SEM (*, $P < 0.05$; **, $P < 0.01$; ***, $P < 0.001$; and ****, $P < 0.0001$).

increased Treg ($CD4^+FoxP3^+$) presence in the blood and no significant difference in the TME, consistent with our previous report (5). However, consistent with our previous results (5), entinostat treatment resulted in a significant decrease in the protein levels of FoxP3 in the circulating $CD4^+FoxP3^+$ cells (Fig. 2A; Supplementary Fig. S1). The combination group,

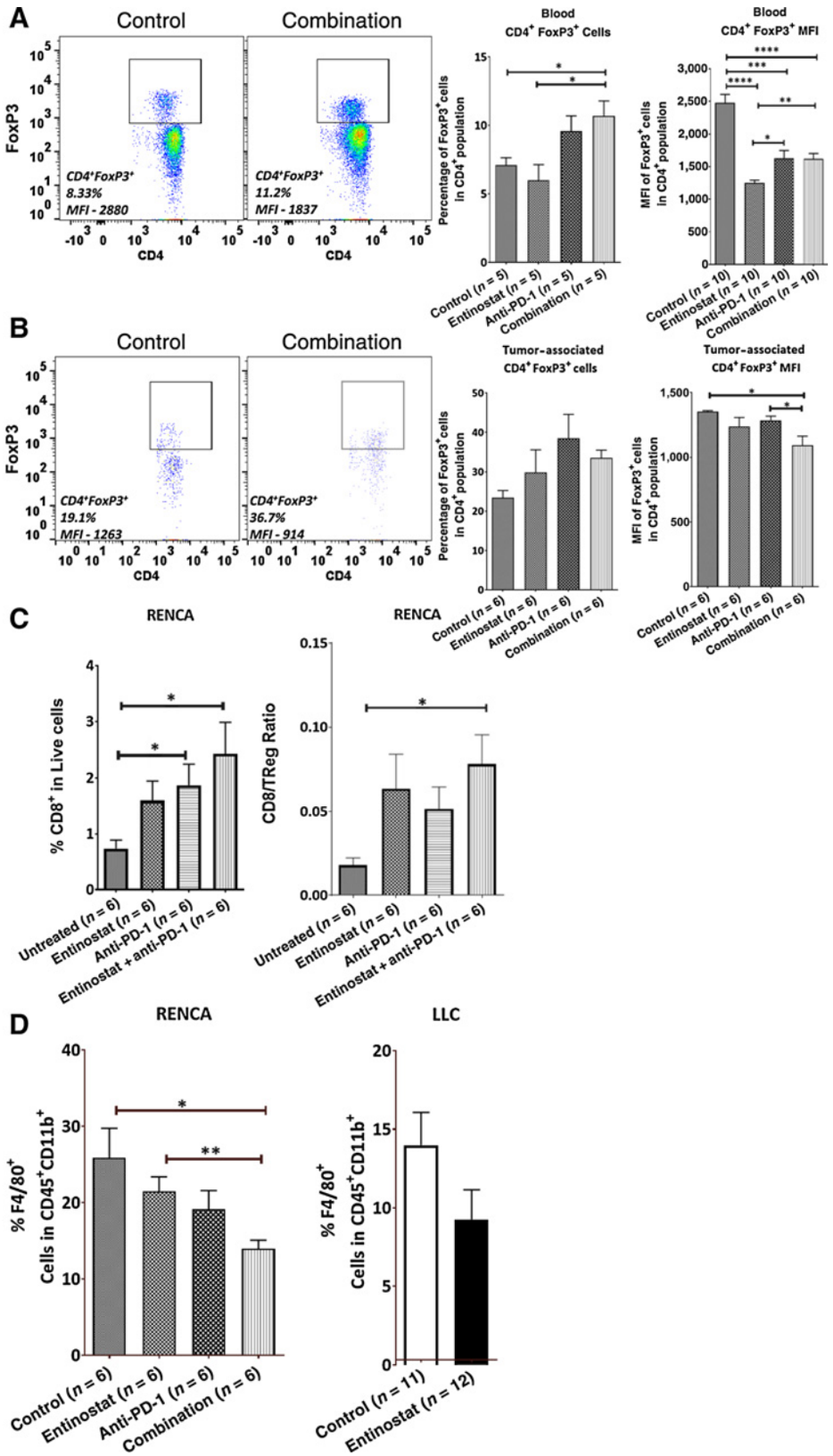

Figure 2.

Entinostat modulates T-cell and TAM response in the RENCA and LLC models. Blood and tumor samples were isolated from mice at the end of the study and processed for flow cytometry analysis. **A,** Left, FACS analysis of blood shows the effect of vehicle and combination treatment on CD4 and FoxP3 levels. Right, Quantification of Treg presence in the blood and protein expression shown as mean fluorescence intensity (MFI). **B,** Left, FACS analysis of tumor-cell suspensions from RENCA mice after control or entinostat treatment. Right, Quantification of Treg presence in the TME and protein expression shown as MFI. **C,** Quantitative FACS analysis of $CD8^+$ T-cell infiltrates into the TME. **D,** Left, Quantitative FACS analysis results of TAM infiltration into the TME. $n = 3$–5 tumors/blood samples per cohort per panel. Right, LLC tumor–bearing mice were orally treated with vehicle (1% DMSO) or entinostat solution (10 mg/kg) for 2 weeks. Tumor cells were processed and analyzed by flow cytometric analysis. Results are shown as mean ± SEM (*, $P < 0.05$; **, $P < 0.01$; ***, $P < 0.001$; and ****, $P < 0.0001$).

while also showing a significant reduction in FoxP3 protein levels as compared with the control group, did not show reduced FoxP3 levels relative to entinostat alone (Fig. 2A and B). In the TME, entinostat did not affect expression of FoxP3. A very modest, albeit significant, reduction in the MFI of $CD4^+FoxP3^+$ cells was observed in the combination treatment group (Fig. 2B), suggesting that an inhibition of Treg function associated with decreased expression of FoxP3 protein (17, 18) could be the result of decreased tumor burden observed in this group rather than a direct effect of entinostat.

$CD8^+$ T cells are affected by the PD-1/PD-L1 axis and are crucial to tumor surveillance. When the PD-1/PD-L1 checkpoint axis is blocked, there is often an increase in effector T-cell function and tumor infiltration (19, 20). We found that the combination effect of entinostat and anti–PD-1 immunotherapy resulted in a significant increase in tumor-infiltrating $CD8^+$ T cells (control vs. combination: $P = 0.0352$; Fig. 2C, left; Supplementary Fig. S1). Similarly, we observed a statistically significant increase in the $CD8^+$ T-cell–Treg ratio, suggesting the generation of a less immunosuppressive environment (control vs. combination: $P = 0.0218$; Fig. 2C, right).

In addition to $FoxP3^+$ Tregs, there are multiple immunosuppressive myeloid cells recruited to the TME including tumor-associated macrophages (TAM) and MDSCs. Upon migration of immature monocytic cells to the tumor, these cells differentiate to TAMs. These cells are marked by the pan-macrophage marker F4/80 in combination with $CD45^+CD11b^+$ markers. Entinostat alone compared to control caused a modest and not statistically significant reduction in TAMs (Fig. 2D). A significant reduction in TAMs was observed only in the combination group as compared with control and entinostat alone (combination vs. control: $P = 0.0272$; combination vs. entinostat: $P = 0.009$) in the RENCA model, suggesting that these changes may be a consequence of decreased tumor burden observed in this group. Taken together, these results suggest that potentiating effect of entinostat on PD-1 immune therapy was not mediated by changes in Tregs or macrophages in TME.

MDSC function is neutralized by entinostat treatment

MDSCs contribute to the immune-suppressive TME by inhibiting antitumor T-cell immune responses. MDSCs are present in two phenotypically defined subpopulations: granulocytic $CD11b^+Ly6G^+Ly6C^{low}$ (PMN-MDSCs) and monocytic $CD11b^+Ly6C^{high}Ly6G^-$ (M-MDSCs) MDSCs (21). Recent data suggest that phenotype is an important descriptor of MDSCs, but not a sufficient criterion for defining and identifying MDSCs, which requires additional functional characterization of the cells (22). The tumor attracts MDSCs, monocytes, and immature myeloid cells via release of chemoattractants, such as CCL2, CCL5, CCL7, and CXCL12 (8, 22–25). Once in the TME, MDSCs have been shown to promote resistance to $CD8^+$ Teff cells and enhance the immune escape of the tumor via multiple mechanisms including upregulation of surface PD-L1, production of immunosuppressive cytokines (IL10, TGFβ) and Treg-attracting cytokines (CCL4, CCL5), and elevation of arginase-1 (Arg1) and iNOS (23, 24, 26).

Treatment with entinostat alone caused an increase in phenotypically defined PMN-MDSC and M-MDSC within tumors, whereas anti–PD-1 single-agent treatment led to a reduction in the PMN-MDSC populations (Fig. 3A and B; Supplementary Figs. S1 and S2A). The slight increase in MDSC populations observed in the entinostat group was amplified in the combination group (Fig. 3B). We also observed a significant increase in accumulation of splenic PMN-MDSC ($P = 0.0053$) and M-MDSCs ($P = 0.0063$) in the entinostat-treated LLC model (Supplementary Fig. S2B) and PMN-MDSCs ($P = 0.0441$) in the combination-treated RENCA model (Supplementary Fig. S2C). In addition, we observed increases in the bone marrow MDSCs in LLC tumor–bearing mice (Supplementary Fig. S3A). Similar effects of entinostat on upregulation of the population of PMN-MDSC in bone marrow, spleen, and tumors were observed in another tumor model—CT26 colon carcinoma (Supplementary Fig. S3C).

As an increase in immunosuppressive MDSCs was not consistent with the antitumor activity that was observed with either entinostat alone or in combination with anti–PD-1, the functional activity of accumulating MDSCs was examined. We tested *ex vivo* the ability of tumor-associated MDSCs to suppress proliferation of antigen-specific and nonspecific (CD3/CD28-stimulated) $CD8^+$ T cells from tumor-free mice. PMN-MDSC and M-MDSC from tumors of untreated mice showed potent suppressive activity (Fig. 3C–E). In sharp contrast, MDSCs isolated from tumors of entinostat-treated or entinostat/anti–PD-1-treated mice had poor suppressive activity as demonstrated by an inability to inhibit proliferation of stimulated $CD8^+$ T cells (Fig. 3C–E). Importantly, this effect was equally observed in entinostat alone and combination groups. MDSCs from the spleen of LLC tumor–bearing mice also showed a reduced capacity for inhibition of T-cell proliferation in the entinostat-treated cohort (Supplementary Fig. S4A). Further examination of the $CD8^+$ T cells from these coculture experiments revealed increased Granzyme B production by approximately 40% compared with the control group, in which MDSCs from an untreated tumor-bearing mouse were cocultured with prestimulated $CD8^+$ T cells (P value ≤ 0.01 for each condition and MDSC:T-cell ratio; Fig. 3F; Supplementary Fig. S4B). These data indicate that although entinostat alone, and when combined with anti–PD-1, increased intratumor numbers of cells with PMN-MDSC and M-MDSC phenotype, these cells have lost the majority of their immunosuppressive activity.

Entinostat treatment of MDSC-like cell line J774M and LLC isolated MDSCs reveals potential mechanistic targets

The J774M cell line has recently been characterized as a stable MDSC-like cell line (27, 28). To validate these findings for the purposes of our experiments, we stained these cells for Ly6C and Ly6G to confirm the MDSC-like status of the cells. As shown in Fig. 4A, the subpopulation ratio of these cells closely resembles what is found in the RENCA TME. Of the $CD45^+CD11b^+Gr1^+$ populations, approximately 90% of the cells are PMN-MDSC ($Ly6G^+$) and approximately 10% of the cells are M-MDSC ($Ly6C^+$; ref. 29). Following validation of the cell phenotype, we studied the effect of entinostat on the functional alteration of the immunosuppressive capacity of these cells. We treated the cells for up to 48 hours with concentrations ranging from 0.01 to 5 μmol/L of entinostat with no significant impact on J774M cell proliferation or viability (Supplementary Fig. S5A and S5B). Coculture of 0.5 μmol/L entinostat-treated J774M cells with preactivated $CD8^+$ T cells for 68–72 hours revealed a significant increase in $CD8^+$ T-cell proliferation nearing that of $CD8^+$ T cells alone, with minimal additional effect at higher entinostat doses (Fig. 4B,

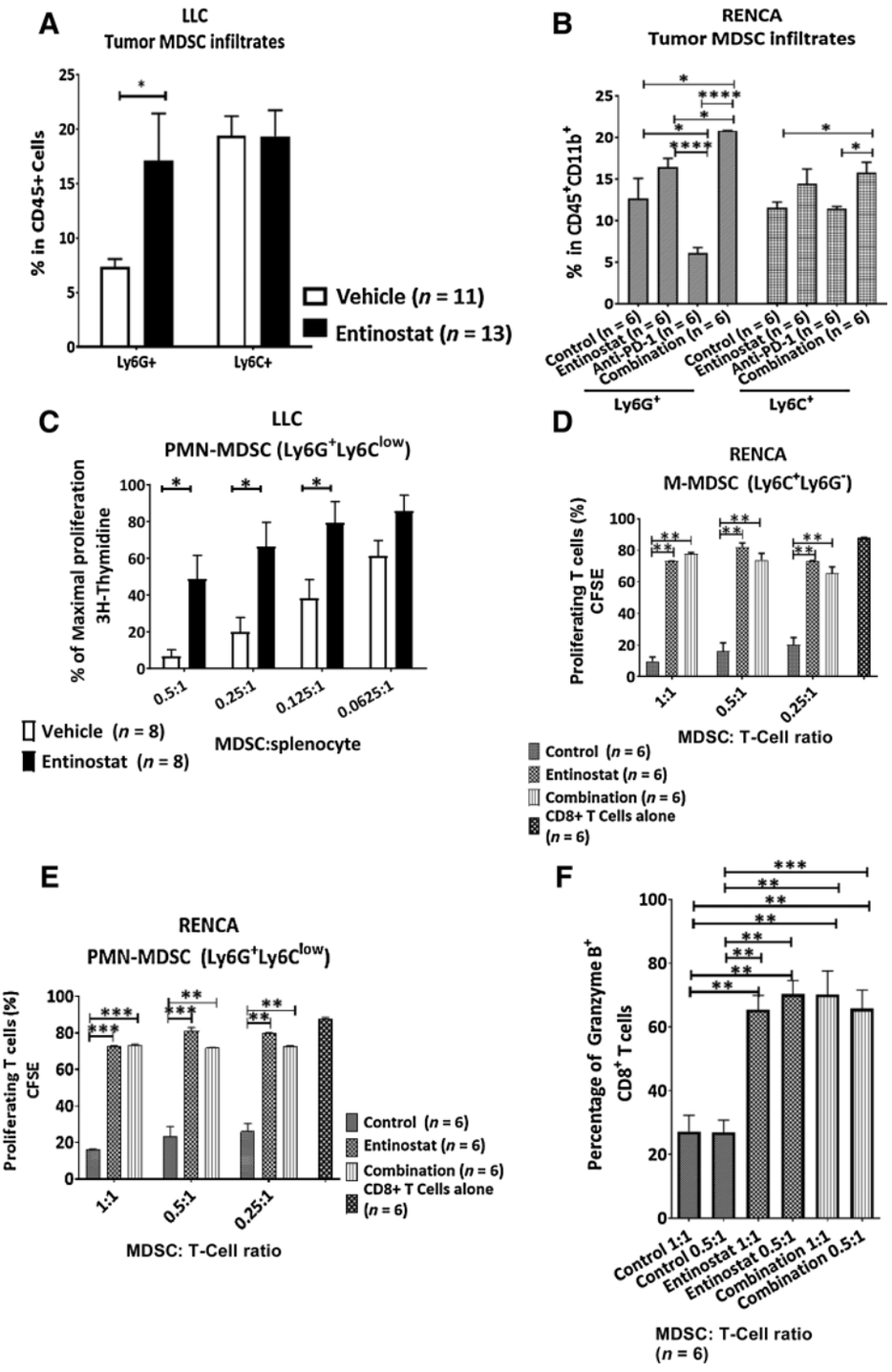

Figure 3.
Entinostat inhibits the immunosuppressive capacity of MDSCs. **A** and **B,** Cells with MDSC phenotype infiltrating LLC (**A**) or RENCA (**B**) tumors in mice treated for 2 to 4 weeks with vehicle (1% DMSO), entinostat, anti–PD-1, or combination. **C,** LLC Ly6G$^+$ cells were enriched by MACS separation from tumor cells and cultured with splenocytes from PMEL mice and 0.1 mg/mL of gp100 peptide for 3 days. Cell proliferation was measured in triplicate using ^{3}H-thymidine uptake. M-MDSC (**D**) and PMN-MDSC (**E**) cells isolated from the RENCA TME were cocultured with CFSE-tagged CD8$^+$ T cells for 16 to 18 hours, at which time they were collected, stained with CD8 and Granzyme B antibodies, and subjected to FACS analysis in triplicate for T-cell proliferation (n = 3–5 tumors). **F,** Quantitative representation of FACS analysis of cytotoxic CD8$^+$ active protein Granzyme B from T cells which have been cocultured with MDSCs from control, entinostat, or combination-treated cohorts. Results are shown as mean ± SEM (*, $P < 0.05$; **, $P < 0.01$; ***, $P < 0.001$; and ****, $P < 0.0001$).

Supplementary Fig. S5C). Our previous work with entinostat treatment of FoxP3$^+$ Tregs demonstrated that inhibition of class 1 HDACs led to acetylation of STAT3 and subsequent inhibition of STAT3 phosphorylation and activation. To determine if entinostat utilized a similar mechanism of STAT3 inhibition in MDSCs, J774M cells were treated for 6 hours with 0.5, 0.75, or 1 μmol/L of entinostat. Via immunoprecipitation of STAT3 and Western blot probing for acetylated lysine, we noted that 0.5 μmol/L of entinostat treatment induced STAT3 acetylation without altering the total presence of STAT3 protein (Fig. 5C).

MDSCs have been shown to express high levels of arg1, COX-2, and iNOS, which are key mediators of the immunosuppressive activity of MDSCs. Further investigation of the J774M and LLC cells revealed a striking inhibition of *arg1* expression in the entinostat-treated cells as compared with the untreated cells

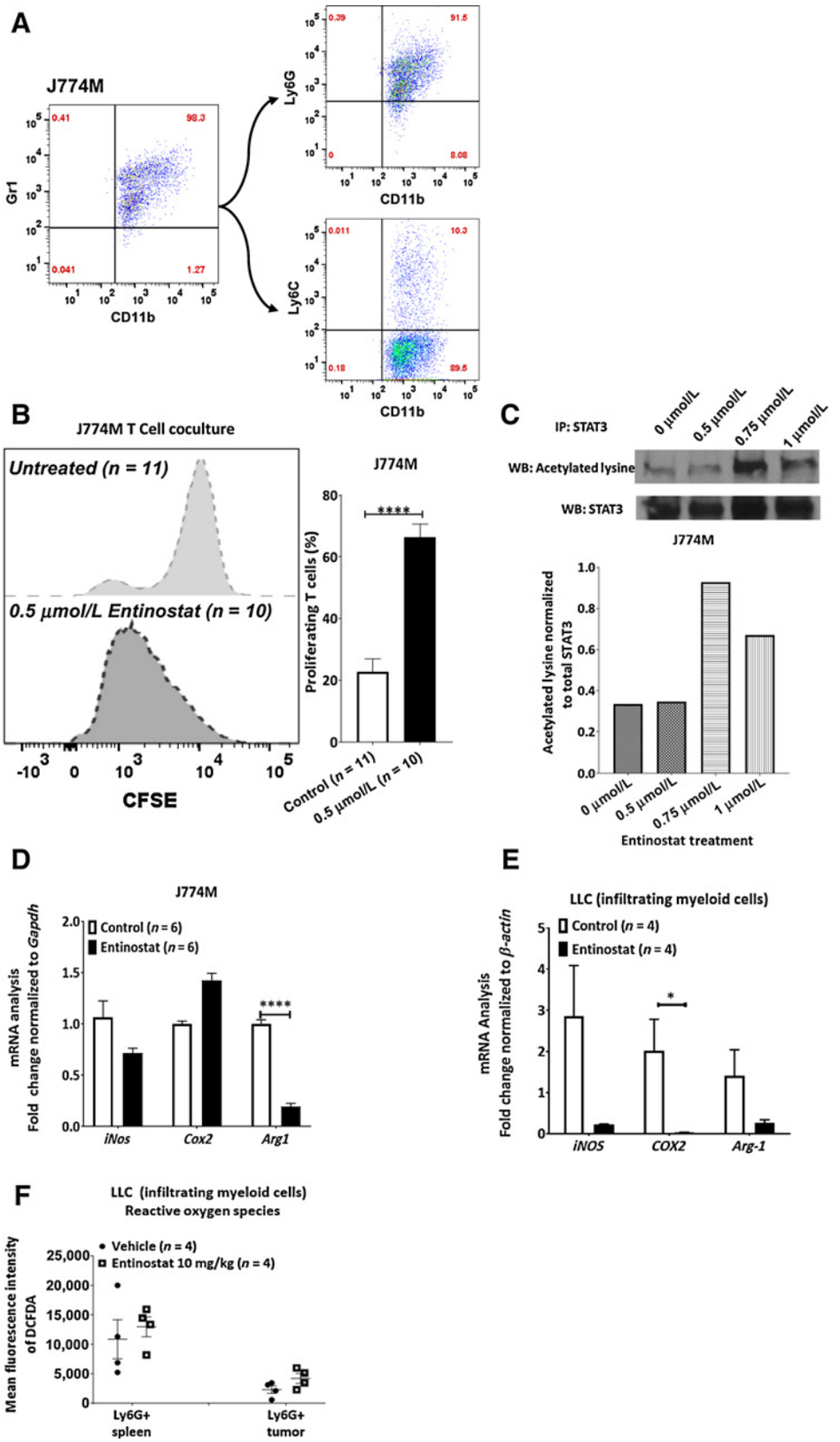

Figure 4.

Entinostat diminishes inhibitory capabilities of MDSC-like cells revealing molecular modifications. **A,** Characteristic FACS analysis of J774M cell line. **B,** Left, CFSE fluorescent histograms of gated $CD8^+$ T cells incubated with J774M cells at a ratio of 1:1. J774M cells were treated with DMSO or 0.5 µmol/L of entinostat. Right, Quantitative representation of **B**. Bars show the mean percentage of proliferating $CD8^+$ T cells. This experiment was repeated 3 times independently. **C,** Entinostat induces acetylation in J774M MDSC-like cells. Cells were treated for 6 hours and then harvested for immunoprecipitation of STAT3 and Western blot staining for acetylated lysine and total STAT3. **D,** Quantitative RT-PCR analysis indicates a significant decrease in key MDSC functional regulator arg1 when J774M cells are treated with entinostat. **E,** Total RNA was extracted from $Ly6G^+$ cells which were enriched from spleen of LLC tumor–bearing mice and analyzed by qRT-PCR. **F,** Spleen and tumor cells were stained with DCFDA and analyzed by flow. Results are shown as mean ± SEM (*, $P < 0.05$; **, $P < 0.01$; ***, $P < 0.001$; and ****, $P < 0.0001$).

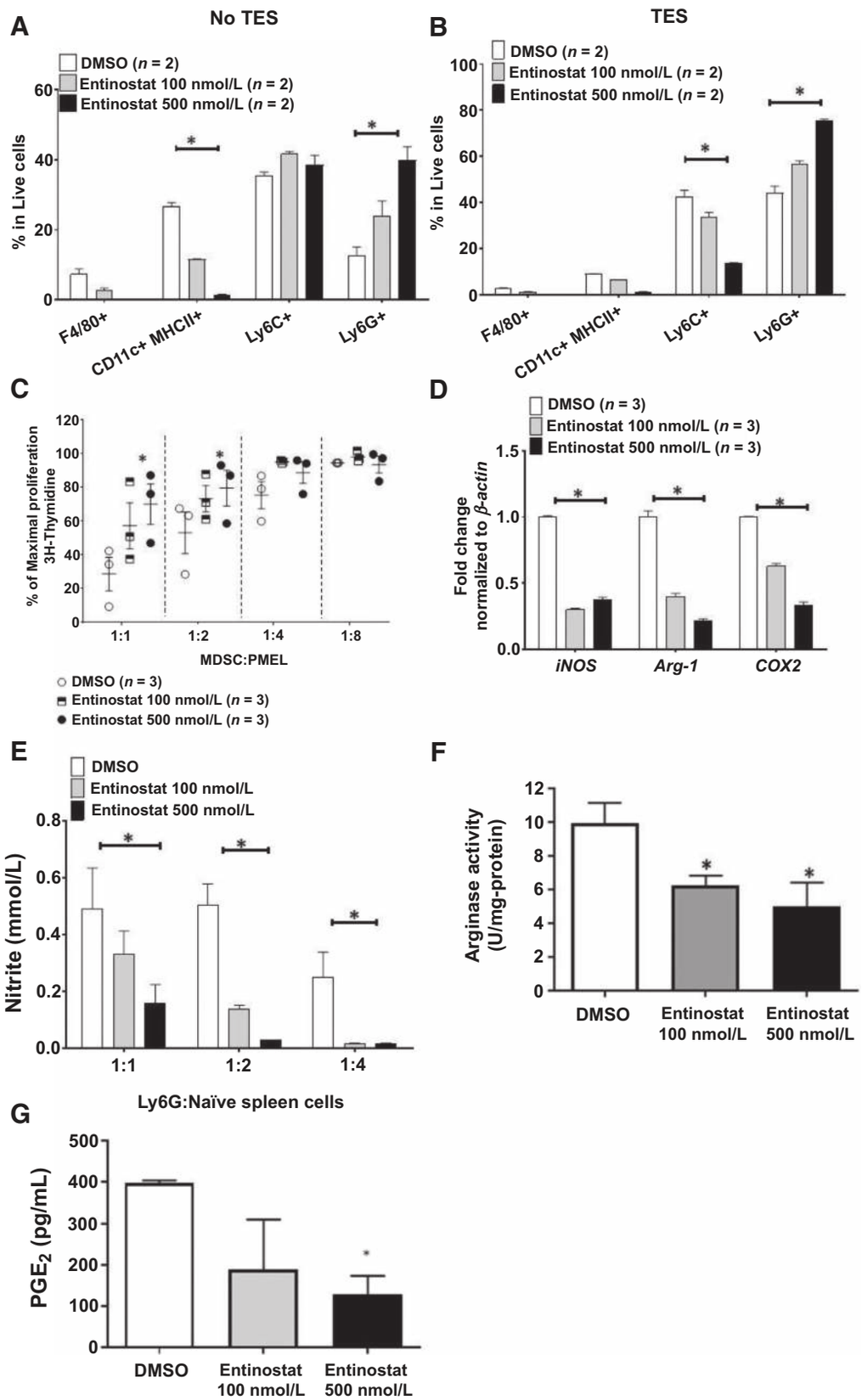

(RENCA—control vs. entinostat-treated: $P = 0.003$; LLC—control vs. entinostat-treated: $P = 0.163$; Fig. 4D and E). Arg1 allows for induction of cell-cycle arrest in the cytotoxic T-cell population *via* arg1 conversion of circulating L-arginine pools to urea and L-ornithine, thus reducing the presence of extracellular L-arginine, which is necessary for cytotoxic T-cell survival (10, 25). Consistent with the effects of entinostat on arg1 expression, further characterization of entinostat-treated J774 and LLC MDSCs revealed reduced expression of *NO* (RENCA—$P = 0.083$; LLC—$P = 0.121$) and *cox2* genes (LLC—$P = 0.041$; Fig. 4D and E). Entinostat did not affect the level of ROS in MDSCs (Fig. 4F). These data indicate that entinostat may directly target STAT3 signaling to impair the T-cell–inhibiting activity of MDSCs, through downregulation of *arg1*, *iNOS*, or *Cox-2*.

Effect of entinostat on differentiation and function of MDSC *in vitro*

Previous data have demonstrated that class 1 HDACs may play a role in the differentiation of myeloid progenitor cells to MDSCs, DCs, and macrophage. To evaluate the effect of entinostat on MDSC differentiation, enriched bone marrow hematopoietic progenitor cells (HPC) from tumor-free mice were cultured with GM-CSF and TES for 6 days in the presence of different concentrations of entinostat. In the absence of TES, entinostat caused a significant decrease in the differentiation of $CD11c^+MHCII^+$ DCs, without affecting $F4/80^+$ macrophages and $Ly6C^{hi}$ monocytes. In contrast, the presence of $Ly6G^+$ granulocytes was significantly increased (Fig. 5A). Entinostat-inducible upregulation of granulocytic, $Ly6G^+$, differentiation was observed during HPC differentiation in the presence of TES. No effect on macrophages, $F4/80^+$, DCs, and $CD11c^+MHCII^+$ was seen. However, the presence of monocytes, $Ly6C^+$, was significantly decreased (Fig. 5B). Thus, consistent with *in vivo* data, entinostat promoted differentiation of granulocytic cells. To assess the effect of entinostat on MDSC-suppressive activity, $Ly6G^+$ cells were isolated after a 6-day HPC culture with different concentrations of entinostat, GM-CSF, and TES, and used in an antigen-specific suppressive assay. PMN-MDSC derived in this manner had potent suppressive activity, which was inhibited in a dose-dependent manner by entinostat (Fig. 5C). Similar to the results obtained *in vivo*, entinostat significantly reduced expression of genes involved in immune suppression in PMN-MDSC: *nos2*, *arg1*, and *cox-2* (Fig. 5D). Downregulation of the expression of *nos2* was associated with decreased production of NO in entinostat-treated cells (Fig. 5E). Reduced expression of *arg1*, was associated with decreased arginase activity (Fig. 5F). MDSC-derived prostaglandin E2 (PEG2) was significantly reduced with entinostat treatment (Fig. 5G). Thus, the effect of entinostat on PMN-MDSC generated from HPCs fully recapitulated the effect seen *in vivo*.

Entinostat treatment primes the TME for enhanced response to immunotherapy

To examine the effect of entinostat on the TME, we subjected tumor samples from control, entinostat, and combination-treated cohorts to a proteome profiler analysis (Ary028) that provided a readout of 111 chemokines and cytokines (Supplementary Fig. S6). Within this pool, we observed a significant decrease in MDSC activation cytokines, including G-CSF ($P \leq 0.001/0.01$), GM-CSF ($P \leq 0.05/0.001$), IL1β ($P \leq 0.001/0.01$), and IL10 ($P \leq 0.001$) in the TME of both the entinostat and combination cohorts relative to the control (Fig. 6A and B). In addition, we observed a significant increase in MDSC-associated trafficking/accumulation cytokines, including IL6 ($P \leq 0.05$) and VEGF ($P \leq 0.01$), in combination cohort relative to the control (Fig. 6C and D). We also noted a significant upregulation of antitumor chemokines and cytokines, which contribute to pro-MDSC inhibition (IL1ra: $P \leq 0.01/0.0001$; ref. 30) and innate antitumor response (IL4: $P \leq 0.001/0.01$ and IL12p40: $P \leq 0.01/0.05$; Fig. 6C and D). These results suggest that entinostat treatment is sufficient to alter the immune profile of the TME toward an antitumor status that may prime the TME to better respond to immunotherapeutic interventions, such as anti–PD-1 treatment. For these data on entinostat treatment priming the host immune system, we subjected serum samples from the control- and entinostat-treated mice to the same Ary028 proteome profiler. We observed significant decreases in multiple, circulating pro–tumor-associated chemokines and cytokines between the control- and entinostat-treated cohorts (Supplementary Fig. S7; Fig. 6E).

Figure 5.

Effect of entinostat on factors involved in PMN-MDSC–mediated suppression in $Ly6G^+$ generated from HPC. **A** and **B,** Lineage-negative cells were enriched from bone marrow cells of naïve female C57BL/6 mice and cultured in RPMI supplemented with 10% FBS, penicillin and streptomycin, and 20 ng/mL of GM-CSF at 50,000 cells/well in 24-well plates. On day 1, TES or media with DMSO and 100 or 500 nmol/L of entinostat were added into the wells at 10%. On day 3, half of culture supernatant was exchanged to fresh media supplemented with 20 ng/mL of GM-CSF with or without TES. On day 6, cells were collected and analyzed by flow cytometric analysis. Results represent mean ± SEM of duplicate (*, $P < 0.05$). **C,** HPC cells from naïve bone marrow cells were cultured with 20 ng/mL of GM-CSF, 10% of TES, and DMSO or entinostat for 6 days. $Ly6G^+$ cells were enriched by MACS separation and cocultured with splenocytes from PMEL mice and 0.1 mg/mL of gp100 peptide for 3 days. Cell proliferation was measured in triplicate using ^{3}H-thymidine uptake. Results represent mean ± SEM of two independent experiments. **D,** HPC cells from naïve bone marrow cells were cultured with 20 ng/mL of GM-CSF, 10% of TES, and DMSO or entinostat for 6 days. $Ly6G^+$ cells were enriched by MACS separation. RNA was extracted from $Ly6G^+$ cells and analyzed by qRT-PCR. Data represent mean ± SEM of triplicate, and statistically analyzed by Tukey multiple comparisons test (*, $P < 0.05$). **E,** HPC cells from naïve bone marrow cells were cultured with 20 ng/mL of GM-CSF, 10% of TES, and DMSO or entinostat for 6 days. $Ly6G^+$ cells were enriched by MACS separation and cocultured with naïve splenocytes and 0.1 mg/mL of anti-CD3 and anti-CD28 antibodies for 24 hours at 10^5 cells/well. Nitrite concentration in culture supernatant was analyzed by Griess Reagent System (Promega). Data represent mean ± SEM of triplicate, and statistically analyzed by Tukey multiple comparisons test (*, $P < 0.05$). **F,** Arginase activity (*in vitro* HPC). HPC cells from naïve bone marrow cells were cultured with 20 ng/mL of GM-CSF, 10% of TES, and DMSO or entinostat for 6 days. $Ly6G^+$ cells were enriched by MACS separation and lysed with lysis buffer of an Arginase activity assay kit (abcam). Arginase activity was measured using an Arginase activity assay kit. Data represent mean ± SEM of duplicated two independent experiments and statistically analyzed by *t* test (*, $P < 0.05$). **G,** PGE2 production in culture supernatant (*in vitro* HPC). HPC cells from naïve bone marrow cells were cultured with 20 ng/mL of GM-CSF, 10% of TES, and DMSO or entinostat for 6 days. $Ly6G^+$ cells were enriched by MACS separation and cultured at 2×10^6 cells/mL in RPMI complete media with 20 ng/mL of GM-CSF for 20 hours. PGE2 concentration in supernatant was measured using the PGE2 ELISA Kit (Invitrogen). Data represent mean ± SEM of duplicate.

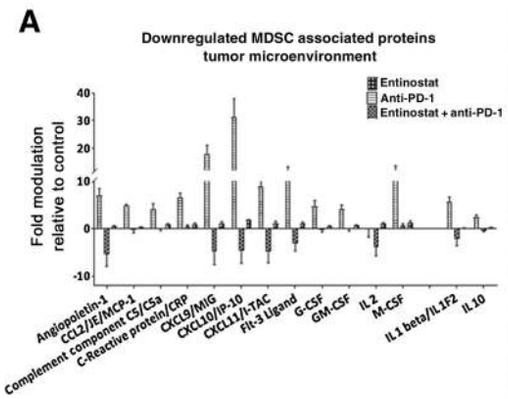

B	Entinostat–Anti-PD-1	Entinostat–combination	Anti-PD-1–combination
Angiopoietin-1	**	**	**
CCL2/JE/MCP-1	****	****	****
Complement Component C5/C5a	*	*	**
C-Reactive Protein/CRP	****	****	****
CXCL9/MIG	***	***	***
CXCL10/IP-10	**	**	**
CXCL11/I-TAC	****	****	**
Flt-3 Ligand	****	****	****
G-CSF	**	**	**
GM-CSF	**	**	**
IL2	ns	ns	ns
M-CSF	*	*	*
IL1 beta/IL1F2	***	*	**
IL10	***	ns	***

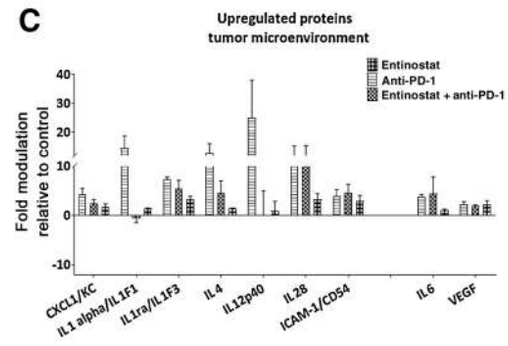

D	Entinostat–Anti-PD-1	Entinostat–combination	Anti-PD-1–combination
CXCL1/KC	ns	ns	ns
IL1 alpha/IL1F1	*	ns	*
IL1ra/IL1F3	***	ns	ns
IL4	**	****	ns
IL12p40	ns	ns	ns
IL28	ns	ns	ns
ICAM-1/CD54	ns	ns	ns
IL6	ns	ns	ns
VEGF	***	**	*

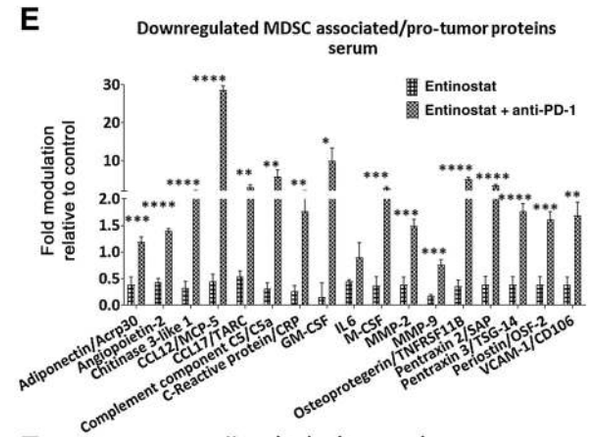

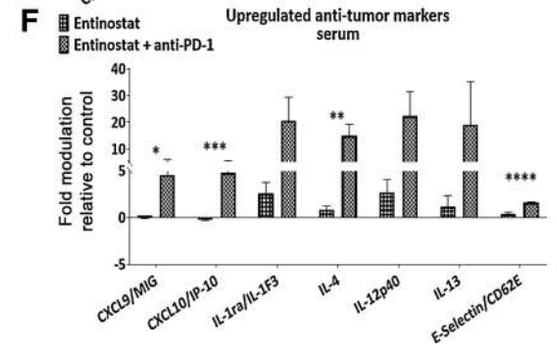

Among these were a MDSC expansion regulator, adiponectin ($P \leq 0.01$); protumor chemoattractant, angiopoietin-2 ($P \leq 0.0001$); inflammation-promoting chitinase 3-like 1 ($P \leq 0.001$), CCL12 ($P \leq 0.01$), complement component C5 ($P \leq 0.01$), c-reactive protein ($P \leq 0.001$), IL6 ($P \leq 0.0001$), pentraxins 2/3 ($P \leq 0.01$), and periostin ($P \leq 0.001$); Treg chemokine, CCL17 ($P \leq 0.001$), MDSC chemoattractants M-CSF ($P \leq 0.01$) and GM-CSF ($P \leq 0.01$); EMT/invasion matrix-metalloproteinases, MMP-2 ($P \leq 0.001$) and MMP-9 ($P \leq 0.0001$); CCL2 ($P \leq 0.01$)—MDSC attractant-inducing osteoprotegerin ($P \leq 0.001$); and leukocyte attractant VCAM ($P \leq 0.001$; Fig. 6E).

Although we did not observe upregulation of antitumor cytokines/chemokines in the entinostat-treated group, there was a significant upregulation of multiple cytokines/chemokines in the combination cohort, suggesting that anti–PD-1 immunotherapy and entinostat work together to enhance the host immune system for improved immunotherapeutic responses (Fig. 6F). We observed increases in the following antitumor-related cytokines/chemokines: T-cell attractants and antiendothelial markers [CXCL9 ($P \leq 0.001$) and CXCL10 ($P \leq 0.0001$)], tumor proliferation inhibitory cytokines [IL4 ($P \leq 0.0001$) and IL13 ($P \leq 0.0001$)], T-cell chemoattractant [E-selectin ($P \leq 0.0001$)], and antitumor marker (IL12p40; $P \leq 0.0001$; Fig. 6F). These results suggest that entinostat treatment alters the host environment and the TME in a manner that allows for enhancement of anti–PD-1 immunotherapy treatment.

Discussion

The recent advancement in the therapeutic approach for patients with solid tumors, including RCC and NSCLC, has been remarkable and driven forward in particular with the emergence of effective and generally well-tolerated immunotherapies showing durable clinical benefit. We are still striving to have these advantageous therapies become effective for a larger population of patients as only 20% to 30% of patients with RCC and NSCLC will have a durable response (1, 2). Our study offers evidence supporting further development of the HDACi entinostat as an effective treatment to combine with immunotherapies.

In this study, we tested the effect of combining a class I–selective HDAC inhibitor, entinostat, with anti–PD-1 immunotherapy in two syngeneic mouse models of RCC and NSCLC along with a series of *in vitro* experiments aimed at characterizing the basis for the enhanced antitumor activity observed for this combination. In addition to delayed tumor growth, we observed that entinostat and anti–PD-1 immunotherapy prolonged survival in our RCC model. Entinostat alone did not affect the presence of Treg or macrophages in TME. However, it caused upregulation of $CD8^+$ T cells (although it did not reach statistical significance). Although combination treatment reduced tumor-associated $FoxP3^+$ and significantly reduced the presence of FoxP3 protein in the cells, it is difficult to exclude that this was the result of significantly reduced tumor burden in these mice. However, these findings support the hypothesis that entinostat in combination with immunotherapy treatment, rather than being directly cytotoxic to the tumor, has significant immunomodulatory activity (5, 31).

Recent reports suggest that HDAC inhibition alters the cytokine release and may change the function of innate immune cell infiltrates in the TME (6, 8, 12, 32). Interestingly, correlative studies performed in breast cancer patients receiving entinostat showed a decrease in both monocytic and granulocytic MDSCs (32). In our experimental conditions, we actually observed an increase in both monocytic and granulocytic subsets of the MDSC population. MDSC are well-known inhibitors of T-cell proliferation and activity. Recent reports suggest that HDACs may play a role in this suppressive function (6, 10, 12, 19, 21, 23, 25). Thus, our study shows that entinostat treatment has an inhibitory effect on PMN- and M-MDSC suppressive function both *in vivo* and *in vitro*—either with cells directly from the TME or using an MDSC-like cell line. Additional analysis of MDSCs treated with entinostat revealed a significant inhibition of arg1 activity and NO production as well as *cox2* expression suggesting potential mechanisms of action by which entinostat inhibits the function of the immunosuppressive MDSC populations. It is also intriguing that we observed a reduction of tumor-infiltrating macrophages in the entinostat-treated tumor suggesting a potential role of HDAC inhibition also on the innate immune response.

Entinostat treatment has been associated with altered inflammatory responses via cytokine/chemokine release and trafficking (33–35). Such circulating proteins affect the function and response of the immune system to disease. The release of chemoattractants from the TME is necessary for immune infiltration

Figure 6.

Treatment with entinostat significantly alters the highly immunosuppressive environment found in RENCA tumors. Tumor and blood samples collected from mice at the end of the study were processed and examined using the Proteome Profiler Mouse XL Cytokine array Kit (Ary028). **A,** Quantification of fold change relative to the control cohort of MDSC associated or protumor cytokines/chemokines which were significantly downregulated in the presence of entinostat. Control cohort mean pixel density values: angiopoietin-1: 455.08; CCL2/JE/MCP-1: 652.64; Complement Component C5/C5a: 1887.40; C-Reactive protein: 1297.67; CXCL9/MIG: 585.36; CXCL10/IP-10: 101.88; CXCL11/I-TAC: 453.05; Flt-3 Ligand: 354.88; G-CSF: 761.15; GM-CSF: 673.24; IL2: 359.52; M-CSF: 1544.22; ILbeta/IL1F2: 324.43; IL10: 2679.17. **B,** Statistical significance quantification between groups in **A**. **C,** Quantification of fold change relative to the control cohort of antitumor chemokines/cytokines which were upregulated significantly in the presence of entinostat treatment. Control cohort mean pixel density values: CXCL1/KC: 1613.03; IL1alpha/IL1F1: 388.22; IL1ra: 1637.52; IL4: 512.23; IL12p40: 133.11; IL28: 2467.05; ICAM-1/CD54: 9548.49; IL6: 319.05; VEGF: 10333.375. **D,** Statistical significance quantification between groups in **C**. **E,** Ary028 array fold change results from serum samples of entinostat and combination-treated mice relative to the control cohort ($n = 2$ samples/cohort and 3 data points per tumor). Control cohort mean pixel density values: Adiponectin/ACRP30: 18200.68; Angiopoietin-2: 18961.915; Chitinase 3-like 1: 9533.66; CCL12/MCP-5: 846.13; CCL17/TARC: 902.46; Complement C5/C5a: 1456.19; C-reactive protein/CRP: 12122.46; GM-CSF: 165.95; IL6: 471.48; M-CSF: 4491.38; MMP-2: 14329.05; MMP-9: 17967.9; Osteoprotegerin/TNFRSF11B: 667.93; Pentraxin 2/SAP: 3923.15; Pentraxin 3/TSF-14: 11726.05; Periostin/OSF-2: 11451.54; VCAM-1/CD106: 9820.95. **F,** Array results showing fold change of entinostat and combination cohorts relative to the control cohort. Control cohort mean pixel density values: CXCL9/MIG: 111.17; CXCL10/IP-10: 330.84; IL1ra/IL1F3: 486.28; IL4: 385.15; IL12p40: 320.31; IL13: 89.93; E-Selectin/CD62E: 13656.05 ($n = 2$ samples/cohort and 3 data points per tumor). Results are shown as mean ± SEM (*, $P < 0.05$; **, $P < 0.01$; ***, $P < 0.001$; and ****, $P < 0.0001$), and statistics were calculated using multiple t tests, discovery was determined using the two-stage linear step-up procedure of Benjamini, Krieger, and Yekutieli, with $Q = 1\%$.

and immune surveillance evasion (7, 10, 23, 36). Through this complex interplay of communication signals, tumor cells and their associated immune infiltrates avoid notice of the immune system (Supplementary Fig. S8). Our study shows significant alterations in the communication between the tumor and host environments. Downregulation of immune infiltrate tracking, expansion, activation, and suppression proteins by entinostat suggest that class I HDAC inhibition plays a central role in this effect. Similarly, the upregulation of multiple antitumor proteins in the serum indicates that entinostat may prime the host environment to better respond to immunotherapy.

The treatment of RCC is rapidly evolving with the introduction of immune checkpoint inhibitors. At the moment, the only approved drug targeting the PD-1/PD-L1 axis is nivolumab in the second-line setting, but the results from two randomized phase III clinical trials with novel combinations of immune checkpoint inhibitors are awaited and will likely change the standard of care for RCC in the first-line setting. Our positive results with entinostat and high-dose interleukin 2 (HD-IL2) in patients with RCC are also encouraging and confirm the clinical immunomodulation of this HDAC inhibitor (37). Thus, it is intriguing to speculate that the differential effect of HDAC inhibition on the immune system may be pleiotropic but perhaps also guided by the type of immunotherapy that it is combined with. For example, it is possible that the effect on Treg and MDSC may be different and have a different contribution depending whether we combine entinostat with either HD-IL2 or a PD-1 inhibitor. Furthermore, the different TME across different tumor types (either within RCC or other solid tumors) may differentially sensitize to this therapeutic approach. This hypothesis is clinically relevant as immune checkpoint inhibitors are becoming the standard of care for several solid tumors, and combinations with HDAC inhibitors are being developed and tested in clinical trials, including combinations of entinostat and PD-1/PD-L1 inhibitors in melanoma, breast, lung, and ovarian cancer patients.

In summary, our study suggests a novel mechanism by which HDAC inhibitor entinostat modulates the immune-suppressive TME resulting in an enhanced antitumor effect. Entinostat has potent immunomodulatory activity through inhibition of MDSC function that enhances anti–PD-1-induced antitumor response. These results have direct clinical implications in designing rational combination treatments for clinical trials. A phase I/II clinical trial of combinational HDAC inhibitor and anti–PD-1 has been initiated at our institute to determine the efficacy, objective response rate, and progression-free survival in RCC patients.

Disclosure of Potential Conflicts of Interest

A. Hashimoto is an employee of Daiichi Sankyo Co., Ltd. P. Ordentlich holds ownership interest (including patents) in Syndax Pharmaceuticals. D. Gabrilovich reports receiving other commercial research support from Syndax Pharmaceuticals. No potential conflicts of interest were disclosed by the other authors.

Authors' Contributions

Conception and design: A. Hashimoto, L. Shen, P. Ordentlich, D. Gabrilovich, R. Pili

Development of methodology: A. Orillion, A. Hashimoto, L. Shen, S. Chintala, D. Gabrilovich, R. Pili

Acquisition of data (provided animals, acquired and managed patients, provided facilities, etc.): A. Orillion, A. Hashimoto, N. Damayanti, L. Shen, R. Adelaiye-Ogala, S. Arisa, R. Pili

Analysis and interpretation of data (e.g., statistical analysis, biostatistics, computational analysis): A. Orillion, A. Hashimoto, L. Shen, R. Adelaiye-Ogala, S. Chintala, P. Ordentlich, C. Kao, B. Elzey, D. Gabrilovich, R. Pili

Writing, review, and/or revision of the manuscript: A. Orillion, A. Hashimoto, S. Chintala, P. Ordentlich, B. Elzey, D. Gabrilovich, R. Pili

Administrative, technical, or material support (i.e., reporting or organizing data, constructing databases): A. Orillion, R. Adelaiye-Ogala, R. Pili

Study supervision: D. Gabrilovich, R. Pili

Acknowledgments

This study was in part supported by a research grant from Syndax Pharmaceuticals, Inc. (D. Gabrilovich and R. Pili) and a generous donation from Dr. Richard Turner and Deidre Turner (R. Pili).

The costs of publication of this article were defrayed in part by the payment of page charges. This article must therefore be hereby marked *advertisement* in accordance with 18 U.S.C. Section 1734 solely to indicate this fact.

Received March 15, 2017; revised May 18, 2017; accepted June 12, 2017; published OnlineFirst July 11, 2017.

References

1. Brahmer JR, Tykodi SS, Chow LQ, Hwu WJ, Topalian SL, Hwu P, et al. Safety and activity of anti-PD-L1 antibody in patients with advanced cancer. N Engl J Med 2012;366:2455–65.
2. Topalian SL, Hodi FS, Brahmer JR, Gettinger SN, Smith DC, McDermott DF, et al. Safety, activity, and immune correlates of anti-PD-1 antibody in cancer. N Engl J Med 2012;366:2443–54.
3. Motzer RJ, Escudier B, McDermott DF, George S, Hammers HJ, Srinivas S, et al. Nivolumab versus everolimus in advanced renal-cell carcinoma. N Engl J Med 2015;373:1803–13.
4. Quinn DI, Lara PN Jr. Renal-cell cancer–targeting an immune checkpoint or multiple kinases. N Engl J Med 2015;373:1872–4.
5. Shen L, Ciesielski M, Ramakrishnan S, Miles KM, Ellis L, Sotomayor P, et al. Class I histone deacetylase inhibitor entinostat suppresses regulatory T cells and enhances immunotherapies in renal and prostate cancer models. PLoS One 2012;7:e30815.
6. Shen L, Orillion A, Pili R. Histone deacetylase inhibitors as immunomodulators in cancer therapeutics. Epigenomics 2016;8:415–28.
7. Hanahan D, Weinberg RA. Hallmarks of cancer: the next generation. Cell 2011;144:646–74.
8. Kroesen M, Gielen P, Brok IC, Armandari I, Hoogerbrugge PM, Adema GJ. HDAC inhibitors and immunotherapy: a double edged sword? Oncotarget 2014;5:6558–72.
9. Draghiciu O, Lubbers J, Nijman HW, Daemen T. Myeloid derived suppressor cells-An overview of combat strategies to increase immunotherapy efficacy. Oncoimmunology 2015;4:e954829.
10. Gabrilovich DI, Nagaraj S. Myeloid-derived suppressor cells as regulators of the immune system. Nat Rev Immunol 2009;9:162–74.
11. Youn JI, Kumar V, Collazo M, Nefedova Y, Condamine T, Cheng P, et al. Epigenetic silencing of retinoblastoma gene regulates pathologic differentiation of myeloid cells in cancer. Nat Immunol 2013;14:211–20.
12. Rosborough BR, Castellaneta A, Natarajan S, Thomson AW, Turnquist HR. Histone deacetylase inhibition facilitates GM-CSF-mediated expansion of myeloid-derived suppressor cells in vitro and in vivo. J Leukoc Biol 2012;91:701–9.
13. Kim K, Skora AD, Li Z, Liu Q, Tam AJ, Blosser RL, et al. Eradication of metastatic mouse cancers resistant to immune checkpoint blockade by suppression of myeloid-derived cells. Proc Natl Acad Sci U S A 2014;111:11774–9.

14. James BR, Anderson KG, Brincks EL, Kucaba TA, Norian LA, Masopust D, et al. CpG-mediated modulation of MDSC contributes to the efficacy of Ad5-TRAIL therapy against renal cell carcinoma. Cancer Immunol Immunother 2014;63:1213–27.
15. Lechner MG, Karimi SS, Barry-Holson K, Angell TE, Murphy KA, Church CH, et al. Immunogenicity of murine solid tumor models as a defining feature of in vivo behavior and response to immunotherapy. J Immunother 2013;36:477–89.
16. Sgambato A, Casaluce F, Sacco PC, Palazzolo G, Maione P, Rossi A, et al. Anti PD-1 and PDL-1 immunotherapy in the treatment of advanced non-small cell lung cancer (NSCLC): a review on toxicity profile and its management. Curr Drug Saf 2016;11:62–8.
17. Kwon H-S, Lim HW, Wu J, Schnoelzer M, Verdin E, Ott M. Three novel acetylation sites in the Foxp3 transcription factor regulate the suppressive activity of regulatory T cells. J Immunol 2012;188:2712–21.
18. Song X, Li B, Xiao Y, Chen C, Wang Q, Liu Y, et al. Structural and biological features of FOXP3 dimerization relevant to regulatory T cell function. Cell Rep 2012;1:665–75.
19. Gajewski TF, Schreiber H, Fu YX. Innate and adaptive immune cells in the tumor microenvironment. Nat Immunol 2013;14:1014–22.
20. Hadrup S, Donia M, Thor Straten P. Effector CD4 and CD8 T cells and their role in the tumor microenvironment. Cancer Microenviron 2013; 6:123–33.
21. Youn JI, Collazo M, Shalova IN, Biswas SK, Gabrilovich DI. Characterization of the nature of granulocytic myeloid-derived suppressor cells in tumor-bearing mice. J Leukoc Biol 2012;91:167–81.
22. Bronte V, Brandau S, Chen SH, Colombo MP, Frey AB, Greten TF, et al. Recommendations for myeloid-derived suppressor cell nomenclature and characterization standards. Nat Commun 2016;7:12150.
23. Marvel D, Gabrilovich DI. Myeloid-derived suppressor cells in the tumor microenvironment: expect the unexpected. J Clin Invest 2015; 125:3356–64.
24. Lu T, Ramakrishnan R, Altiok S, Youn JI, Cheng P, Celis E, et al. Tumor-infiltrating myeloid cells induce tumor cell resistance to cytotoxic T cells in mice. J Clin Invest 2011;121:4015–29.
25. Lu T, Gabrilovich DI. Molecular pathways: tumor-infiltrating myeloid cells and reactive oxygen species in regulation of tumor microenvironment. Clin Cancer Res 2012;18:4877–82.
26. Kumar V, Patel S, Tcyganov E, Gabrilovich DI. The nature of myeloid-derived suppressor cells in the tumor microenvironment. Trends Immunol 2016;37:208–20.
27. Liu F, Li X, Lu C, Bai A, Bielawski J, Bielawska A, et al. Ceramide activates lysosomal cathepsin B and cathepsin D to attenuate autophagy and induces ER stress to suppress myeloid-derived suppressor cells. Oncotarget 2016;7:83907–25.
28. Lu C, Redd PS, Lee JR, Savage N, Liu K. The expression profiles and regulation of PD-L1 in tumor-induced myeloid-derived suppressor cells. OncoImmunology 2016;5:e1247135.
29. Youn JI, Nagaraj S, Collazo M, Gabrilovich DI. Subsets of myeloid-derived suppressor cells in tumor-bearing mice. J Immunol 2008;181: 5791–802.
30. Lewis AM, Varghese S, Xu H, Alexander HR. Interleukin-1 and cancer progression: the emerging role of interleukin-1 receptor antagonist as a novel therapeutic agent in cancer treatment. J Transl Med 2006;4:48.
31. Kato Y, Yoshimura K, Shin T, Verheul H, Hammers H, Sanni TB, et al. Synergistic in vivo antitumor effect of the histone deacetylase inhibitor MS-275 in combination with interleukin 2 in a murine model of renal cell carcinoma. Clin Cancer Res 2007;13(15 Pt 1):4538–46.
32. Tomita Y, Lee MJ, Lee S, Tomita S, Chumsri S, Cruickshank S, et al. The interplay of epigenetic therapy and immunity in locally recurrent or metastatic estrogen receptor-positive breast cancer: correlative analysis of ENCORE 301, a randomized, placebo-controlled phase II trial of exemestane with or without entinostat. Oncoimmunology 2016;5: e1219008.
33. Zheng H, Zhao W, Yan C, Watson CC, Massengill M, Xie M, et al. HDAC inhibitors enhance T-cell chemokine expression and augment response to PD-1 immunotherapy in lung adenocarcinoma. Clin Cancer Res 2016; 22:4119–32.
34. Cantley MD, Fairlie DP, Bartold PM, Marino V, Gupta PK, Haynes DR. Inhibiting histone deacetylase 1 suppresses both inflammation and bone loss in arthritis. Rheumatology (Oxford) 2015;54:1713–23.
35. Cantley MD, Haynes DR. Epigenetic regulation of inflammation: progressing from broad acting histone deacetylase (HDAC) inhibitors to targeting specific HDACs. Inflammopharmacology 2013;21:301–7.
36. Beury DW, Carter KA, Nelson C, Sinha P, Hanson E, Nyandjo M, et al. Myeloid-derived suppressor cell survival and function are regulated by the transcription factor Nrf2. J Immunol 2016;196:3470–8.
37. Pili R, Quinn DI, Hammers HJ, Monk P, George S, Dorff TB, et al. Immunomodulation by HDAC inhibition: results from a phase II study with entinostat and high-dose interleukin 2 in renal cell carcinoma patients (CTEP#7870). Presented at: 2016 Genitourinary Cancers Symposium; January 7-9, 2016; San Francisco, CA. Abstract 500.